



Article

# Influence of Sintering Additives on Modified (Ba,Sr)(Sn,Ti)O<sub>3</sub> for Electocaloric Application

Zhengyu Li \* , Christian Molin and Sylvia E. Gebhardt

Fraunhofer Institute for Ceramic Technologies and Systems IKTS, Winterbergstrasse 28, 01277 Dresden, Germany  
\* Correspondence: zhengyu.li@ikts.fraunhofer.de; Tel.: +49-351-2553-7303

**Abstract:** This paper reports on the influence of sintering additives CuO and MgO on the recently developed lead-free electrocaloric (EC) material Ba<sub>0.82</sub>Sr<sub>0.18</sub>Sn<sub>0.065</sub>Ti<sub>0.935</sub>O<sub>3</sub> (BSSnT-18-6.5). Details on the sintering behavior and the resulting microstructure of bulk ceramic samples prepared through solid-state synthesis and their dielectric, ferroelectric, and electrocaloric properties are presented. On the one hand, the addition of CuO ( $x_{\text{CuO}} = 2\%$ ) significantly reduced the sintering temperature from 1400 °C to 1150 °C. On the other hand, the addition of MgO ( $x_{\text{MgO}} = 1\%$ ) dramatically reduced the average grain size from 40 μm to 0.4 μm, leading to an increase in dielectric breakdown strength from 4.4 V μm<sup>-1</sup> to 7.7 V μm<sup>-1</sup>. Thus, BSSnT-18-6.5 with the addition of MgO to bulk ceramic samples could achieve maximum EC temperature changes ( $|\Delta T_{\text{EC}}|$ ) of 0.27 K around 30 °C with almost no aberration within a broad temperature range from 5 °C to 50 °C under an applied electric field change of 5 V μm<sup>-1</sup>. The results show the potential of this material for the fabrication of multilayer ceramic (MLC) components for future electrocaloric applications.

**Keywords:** lead-free; electrocaloric; sintering additives; dielectric breakdown strength



**Citation:** Li, Z.; Molin, C.; Gebhardt, S.E. Influence of Sintering Additives on Modified (Ba,Sr)(Sn,Ti)O<sub>3</sub> for Electocaloric Application. *Inorganics* **2023**, *11*, 151. <https://doi.org/10.3390/inorganics11040151>

Academic Editor: Kenneth J.D. MacKenzie

Received: 27 February 2023

Revised: 20 March 2023

Accepted: 30 March 2023

Published: 1 April 2023



**Copyright:** © 2023 by the authors. Licensee MDPI, Basel, Switzerland. This article is an open access article distributed under the terms and conditions of the Creative Commons Attribution (CC BY) license (<https://creativecommons.org/licenses/by/4.0/>).

## 1. Introduction

Electocaloric (EC) materials feature a reversible adiabatic temperature change or isothermal entropy change under the application or withdrawal of an electric field [1]. Over the past decade, many efforts have been made to investigate alternative cooling technologies based on solid-state cooling utilizing caloric effects such as the EC effect. Promising materials for electocaloric applications should possess large entropy changes, low hysteresis losses and high dielectric strength to achieve large EC temperature changes in their intended working range [2,3].

It is known that the EC properties, among others, are determined by the applied electric field strength, chemical composition, and microstructure characteristics, such as grain size, the amount of porosity and pore distribution [4]. Among them, the influence of grain size on EC properties has been widely reported. Patel and Kumar found the highest electrocaloric effect (ECE) for a grain size of 0.5 μm in BaTiO<sub>3</sub>-based ceramics, which was the highest grain size within their investigations [5]. Kartashev et al. compared the ECE of nanoceramic (grain size: 0.1–0.4 μm) and microceramic (grain size: 30–50 μm) BaTiO<sub>3</sub>. They found a 2.4-fold higher ECE for microceramics [6]. For 1-x Pb(Mg<sub>1/3</sub>Nb<sub>2/3</sub>)O<sub>3</sub>–x PbTiO<sub>3</sub> (PMN-PT) materials, the highest ECEs were determined for the grain sizes of 2.2 μm [7] and 5.8 μm [8] depending on the PbTiO<sub>3</sub> content.

In the past decades, lead-containing material systems have attracted intensive attention due to their outstanding electrocaloric properties, such as Pb<sub>0.89</sub>La<sub>0.11</sub>(Zr<sub>0.7</sub>Ti<sub>0.3</sub>)<sub>0.9725</sub>O<sub>3</sub> (PLZT) [9], PbSc<sub>0.5</sub>Ta<sub>0.5</sub>O<sub>3</sub> (PST) [10] and 0.92 Pb(Mg<sub>1/3</sub>Nb<sub>2/3</sub>)O<sub>3</sub>–0.08 PbTiO<sub>3</sub> (PMN-8PT) [11]. However, the toxic nature of lead has further raised the growing concern recently. In particular, the cumulative toxicity of lead damages multiple body systems and is especially harmful to children [12]. The accumulation of lead usually comes from pollution during lead mining and processing as well as the machining of lead-based

piezoceramics and electronic waste. Legislation has been introduced in many countries to minimize the amount of lead that enters the environment at the end-of-life of electrical and electronic devices. For example, the EU's Restriction of Hazardous Substances in Electrical and Electronic Equipment (RoHS), revised in 2011, restricts the content of lead to 0.1 wt% in homogeneous materials [13]. In this context, the development of lead-free materials with high electrocaloric effect becomes urgent and necessary. The most investigated lead-free material systems reported in the literature are based on ferroelectric BaTiO<sub>3</sub> as well as relaxor ferroelectrics Bi<sub>0.5</sub>Na<sub>0.5</sub>TiO<sub>3</sub> and K<sub>0.5</sub>Na<sub>0.5</sub>O<sub>3</sub>. The substitution of ions such as Ca<sup>2+</sup> and Sr<sup>2+</sup> on the A site or Zr<sup>4+</sup>, Sn<sup>4+</sup>, and Hf<sup>4+</sup> on the B site of BaTiO<sub>3</sub>, can be used to broaden the temperature range of a large ECE or to shift the maximum of the ECE to the desired temperature. For instance, 0.9 Ba(Ti<sub>0.89</sub>Sn<sub>0.11</sub>)O<sub>3</sub>–0.1 (Ba<sub>0.7</sub>Ca<sub>0.3</sub>)TiO<sub>3</sub> (BTS-10BCT) exhibits a broad ECE peak of more than 0.4 K in the temperature range from 20 °C to 90 °C under an electric field of 4 V μm<sup>-1</sup> [14]. 0.92 Bi<sub>0.5</sub>Na<sub>0.5</sub>TiO<sub>3</sub>–0.08 BaTiO<sub>3</sub> (NBT-8BT) investigated by Bai et al. shows an abnormal ECE with a negative temperature change of 0.33 K under an electric field of 5 V μm<sup>-1</sup> [15]. The material 0.9 K<sub>0.5</sub>Na<sub>0.5</sub>NbO<sub>3</sub>–0.1 SrZrO<sub>3</sub> (KNN-10SZ) shows the large electrocaloric effect of 1.19 K for 3.5 V μm<sup>-1</sup> at 94 °C [16]. Additionally, Sr<sub>0.6</sub>Ba<sub>0.4</sub>Nb<sub>2</sub>O<sub>6</sub> (SBN) shows a maximum electrocaloric temperature change of 0.32 K around 90 °C under an electric field of 6 V μm<sup>-1</sup> [17].

Multilayer ceramic (MLC) components are most promising for EC applications. They can withstand high electric fields, leading to larger EC temperature changes compared to bulk ceramics. Moreover, the adjustable thickness of MLC components can drastically increase cooling capacity compared to thin films while being matched to the system frequency for optimal heat exchange.

In our previous work, we systematically investigated the lead-free ferroelectric material barium titanate (BaTiO<sub>3</sub>) modified with strontium (Sr) and tin (Sn) to achieve a high ECE at room temperature and to simultaneously broaden the temperature range of the ECE [18]. Our results demonstrated that Ba<sub>0.82</sub>Sr<sub>0.18</sub>Sn<sub>0.065</sub>Ti<sub>0.935</sub>O<sub>3</sub> (BSSnT-18-6.5) is a promising candidate for EC applications because of its comparatively high |ΔT<sub>EC</sub>| of 0.49 K around 30 °C even under the application of the low electric field of 2 V μm<sup>-1</sup>. Moreover, it shows a broad ECE peak, |ΔT<sub>EC</sub>| > 0.3 K, in the temperature range from 10 °C to 50 °C. However, the high sintering temperature of 1400 °C combined with the giant grain growth turned out to be challenging for the fabrication of MLC components. High sintering temperatures essentially limit the choice of usable inner electrodes. Thus, the reduction of the sintering temperature can have a positive effect on grain growth and the future manufacturing costs of multilayer components. Additionally, giant grains reduce the dielectric breakdown strength or even promote unwanted electric conductivity paths between the inner electrodes of MLC components. In consequence, BSSnT-18-6.5 components have not been able to withstand high electric fields so far to achieve EC effects comparable to those of lead oxide based materials such as PMN-PT [19,20] or PbSc<sub>0.5</sub>Ta<sub>0.5</sub>O<sub>3</sub> (PST) [21]. The dielectric breakdown strength of dielectric ceramics is strongly dependent on the grain size. Tunkasiri and Rujijanagul described the relationship between the dielectric breakdown strength and grain size of barium titanate by  $E \propto G^{-a}$ , where  $E$ ,  $G$  and  $a$  are the breakdown field strength, the grain size and a constant of the value of approximately 0.5, respectively [22]. This means that the dielectric strength of ceramic components increases with decreasing grain size. Cai et al. introduced a phase-field model to study the dielectric breakdown strength of nanostructured ferroelectric ceramics and also observed an increased dielectric strength in smaller grain-sized ceramics which is attributed to the larger amount of grain boundaries [23]. Both, sintering temperature and grain growth can be influenced using sintering additives. It is known that the addition of CuO lowers the sintering temperature in BaTiO<sub>3</sub>-based materials through the formation of a liquid phase during sintering [24,25]. The addition of MgO can be used to prevent grain growth by the inhibition of the interdiffusion of grains during sintering [26–28].

In the present work, we investigate the influence of the sintering additives CuO and MgO on the BSSnT-18-6.5 material. We intensively study sintering behavior, microstructure,

dielectric and electrocaloric properties with the objective of the future fabrication of lead-free MLC component which possess high dielectric strength and thus high EC temperature changes around room temperature.

## 2. Experimental Procedure

$\text{Ba}_{0.82}\text{Sr}_{0.18}\text{Sn}_{0.065}\text{Ti}_{0.935}\text{O}_3$  (BSSnT-18-6.5) ceramic powders were synthesized by a conventional solid-state reaction. A stoichiometric mixture of  $\text{BaCO}_3$  (Solvay S.A., Duisburg, Germany, 99.86%),  $\text{SrCO}_3$  (Alfa Aesar, Karlsruhe, Germany, 99%),  $\text{SnO}_2$  (abcr, Karlsruhe, Germany, 99.9%) and  $\text{TiO}_2$  (Venator Germany GmbH, Duisburg, Germany, 99.5%) was milled in water at 200 rpm for 6 h using a planetary ball mill (Fritsch, Idea-Oberstein, Germany, Pulverisette 5). The mixed powders were subsequently dried, sieved and calcined in an alumina crucible at 1100 °C for 4 h. Different ratios of sintering additives  $\text{CuO}$  (Merk Group, Darmstadt, Germany, ≥99%) and  $\text{MgO}$  (Merk Group, Darmstadt, Germany, ≥99%) were added to the calcined powders in mole fractions ( $x_i$ ) with respect to the concentrations of BSSnT-18-6.5. The compositions were again ball-milled in isopropanol for 6 h at 200 rpm. A small amount of polyvinyl butyral (TER HELL & CO GMBH, Hamburg, Germany) was added as a binder, and the mixture was dried using a rotary evaporator (BÜCHI Labortechnik AG, Essen, Germany, Rotavapor R-134). The milled powders were then pressed into pellets of a diameter of 10 mm and a thickness of around 1.5 mm. After debinding, the pellets were sintered for 1 h at different temperatures with a heating rate of 5 K min<sup>-1</sup>. After sintering, the samples were of a diameter of 8.4 mm and a thickness of around 1.2 mm. Sintering behavior was characterized by the determination of density (Archimedes' method), weight loss and shrinkage in the lateral dimension. For electrical measurements, the sintered samples were ground to thicknesses between 250 and 800 μm and electrodes of silver conductive paste (Heraeus, Hanau, Germany, C1075SD) were applied. The temperature-dependent relative permittivity and dielectric loss tangent were measured at 0.1 kHz, 1 kHz and 10 kHz in a temperature range from −50 to 150 °C using an LCR meter (Hewlett Packard, HP 4263A). Polarization-electric field ( $P$ - $E$ ) hysteresis loops were measured using a Sawyer Tower circuit with an analog input and digital I/O module (Measurement Computing, USB-1616HS-4). The dielectric breakdown strength was determined using a dielectric strength tester (Sefelec GmbH, Germany, PR 12 PF) by immersing the samples in an insulation fluid (M&I Materials, Midel 7131). Electrocaloric temperature changes were characterized directly in a temperature range from −15 to 95 °C under different magnitudes of electric field using a fine diameter thermocouple (Type K, 50 μm in diameter, Omega Engineering) with a bead-welded junction. For the analysis of the microstructure, micrographs were taken by field emission scanning electron microscopy (FESEM) (Carl Zeiss AG, Germany, ULTRA 55). Average grain sizes were determined by linear analysis by the examination of >500 grains according to the ASTM E112 standard. X-ray diffraction (XRD) measurements were performed at room temperature using a D8 Advance diffractometer (Bruker AXS GmbH, Germany) with a step width of  $\Delta(2\theta) = 0.03^\circ$  and a counting time of 1 s in the range of 10–120°.

## 3. Results

### 3.1. Sintering Behavior

Figure 1 shows the bulk density and shrinkage values of BSSnT-18-6.5 ceramics with different sintering additives. As shown in Figure 1a,b the addition of  $\text{CuO}$  increases the density and reduces the sintering temperature dramatically. By adding  $\text{CuO}$  with a mole fraction of  $x_{\text{CuO}} = 2\%$ , the sintering temperature of BSSnT-18-6.5 could be decreased by 250 K to 1150 °C. This resulted from the formation of the  $\text{Cu}_3\text{TiO}_4$  liquid phase promoting the complete shrinkage and grain growth of the ceramics at lower temperatures [29]. Figure 1c,d depicts the bulk density and shrinkage of BSSnT-18-6.5 with the addition of  $\text{MgO}$  ( $x_{\text{MgO}} = 1\%$ ). The addition of  $\text{MgO}$  has no significant influence on the density and shrinkage of BSSnT-18-6.5. The sintering temperature remains constant at 1400 °C. A

simultaneous addition of CuO ( $x_{\text{CuO}} = 2\%$ ) and MgO ( $x_{\text{MgO}} = 1\%$ ) leads to an increase in density and a reduction in the sintering temperature to 1200 °C.

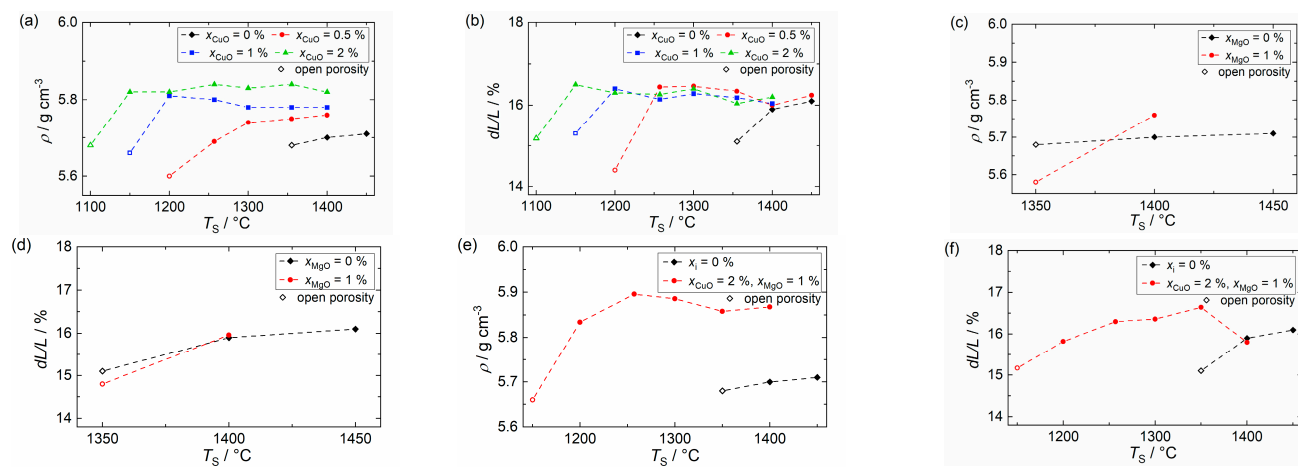


**Figure 1.** Bulk density and shrinkage of BSSnT-18-6.5 bulk ceramics with addition of CuO (a,b), MgO (c,d) and CuO and MgO (e,f).

### 3.2. Microstructural Analysis

The microstructure of sintered bulk ceramics was investigated on selected compositions (Table 1) to evaluate the influence of the addition of MgO and CuO to BSSnT-18-6.5.

**Table 1.** Compilation of samples for further investigations prepared with different mole fractions of CuO ( $x_{\text{CuO}}$ ) and MgO ( $x_{\text{MgO}}$ ) and sintering temperatures ( $T_S$ ).

Sample	$x_{\text{CuO}}/\%$	$x_{\text{MgO}}/\%$	$T_S/^\circ\text{C}$
BSSnT-18-6.5	0	0	1400
BSSnT-Cu	2	0	1150
BSSnT-Mg	0	1	1400
BSSnT-Cu-Mg	2	1	1200

Figure 2a shows the microstructure of BSSnT-18-6.5 with an average grain size of about 40  $\mu\text{m}$ . As shown in Figure 2b, the addition of CuO leads to a bimodal grain size distribution with Cu-rich phases. The accumulation of small matrix grains causes further abnormal grain growth. Due to the resulting coarse grains ( $>10 \mu\text{m}$ ), the addition of CuO is not feasible for the fabrication of multilayer ceramic components. The addition of MgO leads to a homogeneous fine-grained microstructure with an average grain size of 0.4  $\mu\text{m}$  (Figures 2c and 3). The grain size reduction by two orders of magnitude can be explained by our process route, in which MgO was added after calcination. Usually, a replacement of  $\text{Ti}^{4+}$  or  $\text{Sn}^{4+}$  ions by  $\text{Mg}^{2+}$  would lead to the formation of oxygen vacancies up to the solubility limit due to an acceptor-type substitution [30]. By adding MgO after calcination, it is difficult for Mg to solute into the BSSnT-18-6.5 crystal. Hence, the suppression of grain growth can be attributed to the precipitation of Mg at the grain boundary, similarly to the case of Mn doping [31,32].

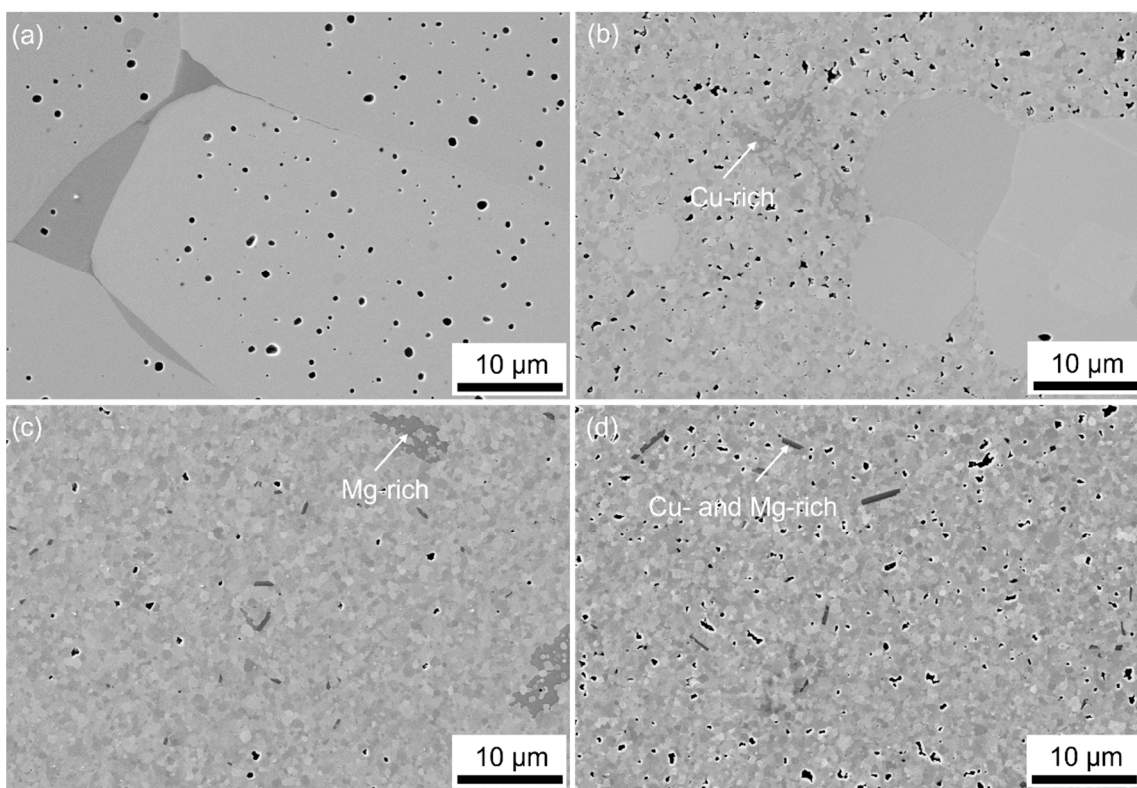


**Figure 2.** FESEM images of BSSnT-18-6.5 (a), BSSnT-Cu (b), BSSnT-Mg (c) and BSSnT-Cu-Mg (d).

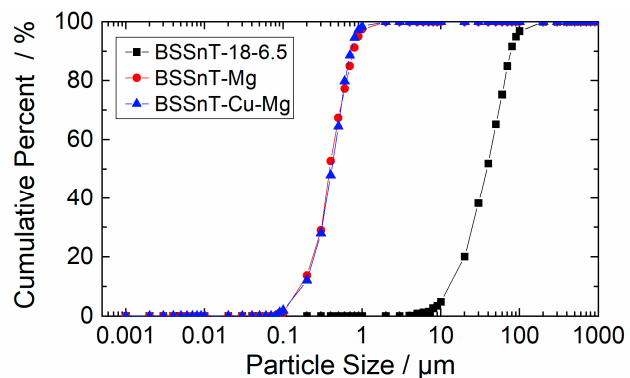


**Figure 3.** Grain size distribution of BSSnT-18-6.5, BSSnT-Mg and BSSnT-Cu-Mg.

Both samples of BSSnT-18-6.5 with sintering additives show an amorphous-like secondary phase which is either Cu-rich (BSSnT-Cu) or Mg-rich (BSSnT-Mg). The simultaneous addition of CuO and MgO results in a monomodal grain size distribution with a fine grain size of 0.4 μm (Figures 2d and 3). Again, secondary phases were observed and were identified as Cu- and Mg-rich phases using dispersive X-ray spectroscopy (EDX). An element mapping analysis of BSSnT-Mg (see Figure S1 in Supplementary Materials) shows the distribution of the different elements Ba, Sr, Ti, Sn, Mg and O.

### 3.3. Phase Analysis

XRD measurements were carried out to determine possible secondary phases within the bulk ceramic samples. The XRD pattern shown in Figure 4 indicates that all samples exhibit a pure perovskite phase without any crystalline secondary phases. The XRD patterns of all compositions are in good agreement with those outlined by the Inorganic Crystal Structure Database for the comparable material composition of  $\text{Ba}_{0.6}\text{Sr}_{0.39}\text{Sn}_{0.26}\text{Ti}_{0.74}\text{O}_3$  (ICSD file no. 01-077-9432), indicating a cubic crystal structure (Pm3m, 211 space group).

The overall shift to lower diffraction angles is due to the difference in the content of Sr and Sn ions, which causes an increase in the lattice parameter.

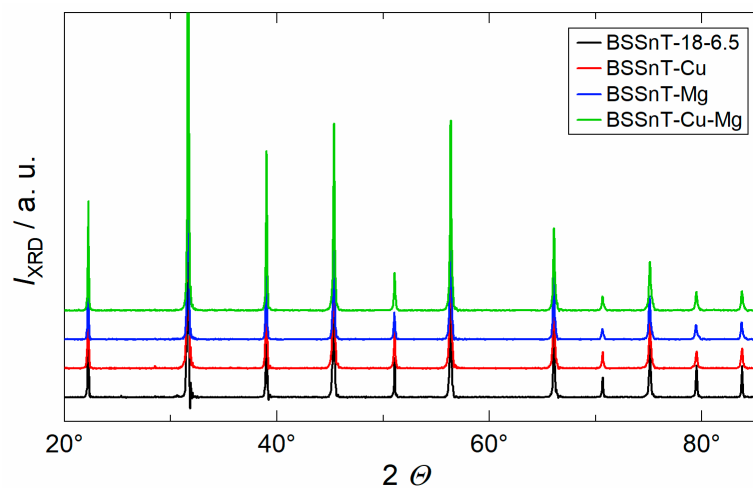


**Figure 4.** X-ray diffraction pattern of sintered BSSnT-18-6.5 ceramics with different additives.

### 3.4. Dielectric Properties

The relative permittivity and dielectric loss as functions of temperature measured at 1 kHz for BSSnT-18-6.5 ceramics with different additives are plotted in Figure 5. BSSnT-18-6.5 shows a permittivity peak at  $T_m = 27^\circ\text{C}$  with a maximum relative permittivity of  $\epsilon_{r,m} = 25,300$ . BSSnT-Cu shows a peak at  $T_m = 19^\circ\text{C}$  with a decreased permittivity of  $\epsilon_{r,m} = 12,900$ . The addition of MgO leads to a broad peak around  $T_m = -11^\circ\text{C}$  and a strongly decreased permittivity of  $\epsilon_{r,m} = 4900$ . The combination of both additives, CuO and MgO, also leads to a broad peak around  $T_m = -1^\circ\text{C}$  with a permittivity of  $\epsilon_{r,m} = 4700$ . All investigated additives reduce the relative permittivity and shift the temperature of maximum permittivity towards lower temperatures. The addition of MgO leads to the largest decrease in  $T_m$ , which is of about 38 K. This reduction can be explained by the reduction in the tetragonal  $c/a$  ratio caused by the local deformation of the perovskite unit cells due to Mg-substitution on the B-sites in the perovskite structure [33].

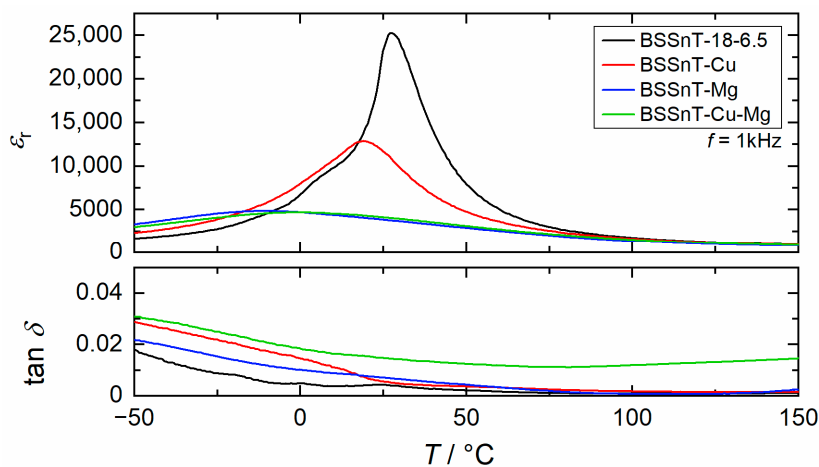


**Figure 5.** Temperature dependence of relative permittivity ( $\epsilon_r$ ) and dielectric loss factor ( $\tan \delta$ ) measured at 1 kHz for BSSnT-18-6.5 ceramics with different additives.

A modified Curie–Weiss law by Uchino and Nomura [34] was applied to calculate the diffuseness parameter of the phase transition:

$$\frac{1}{\varepsilon_r} - \frac{1}{\varepsilon_{r,m}} = \frac{(T - T_m)^\gamma}{C_1}, \quad (T > T_m), \quad (1)$$

where  $\gamma$  and  $C_1$  are modified constants. The exponent  $\gamma = 1$  for an ideal ferroelectric, and  $\gamma = 2$  for an ideal relaxor ferroelectric material. Values of  $1 < \gamma < 2$  indicate an incomplete diffuse phase transition [35]. Figure S2 shows the plots of  $\log(1/\varepsilon_r - 1/\varepsilon_{r,m})$  versus  $\log(T - T_m)$  at 1 kHz for BSSnT-18-6.5 ceramic samples, as well as the slope of their fitting line. The obtained values of  $\gamma$  were found to be in the range of 1.6–1.9 (Table 2), which suggests the occurrence of a diffuse phase transition with both fluctuation-induced disorder in the composition and single or multisite structural disorder in the cationic arrangement in the crystal structure [35]. Moreover, a diffuse phase transition can also be observed in ceramics with small grains and defects [36]. The diffuseness of the phase transition can also be described by an empirical parameter,  $\Delta T_{\text{diffuse}}$ , defined as [37,38]:

$$\Delta T_{\text{diffuse}} = T_{0.9\varepsilon_{r,m}(1 \text{ kHz})} - T_{\varepsilon_{r,m}(1 \text{ kHz})}, \quad (2)$$

where  $T_{0.9\varepsilon_{r,m}(1 \text{ kHz})}$  is the temperature corresponding to 90% of the maximum of the relative permittivity ( $\varepsilon_{r,m}$ ) on the high temperature side at 1 kHz. The values of  $\Delta T_{\text{diffuse}}$  are summarized in Table 2. The results show that MgO addition as well as CuO and MgO addition enhance the diffuseness of the phase transition of BSSnT-18-6.5, which can be explained by the effect of grain size and has long been discovered and discussed in barium titanate systems [39–41]. Furthermore, Mao et al. [42] systematically investigated how a grain size ranging from 0.8 to 8  $\mu\text{m}$  affects the dielectric properties of  $\text{Ba}_{0.7}\text{Sr}_{0.3}\text{TiO}_3$ . They found that ceramics with smaller grains have a broader phase transition than samples with coarser ones, which is caused by the suppression of the phase transition and the consequently reduced relative permittivity. This suppression occurs due to the high amount of low-permittivity and nonferroelectric grain boundaries in fine grain ceramics [43].

**Table 2.** Compilation of temperature of maximum permittivity ( $T_m$ ), maximum relative permittivity ( $\varepsilon_{r,m}$ ), loss factor at  $T_m$  ( $\tan \delta_m$ ), critical exponent ( $\gamma$ ) and empirical parameter ( $\Delta T_{\text{diffuse}}$ ) of BSSnT-18-6.5 with different additives (measured at 1 kHz).

Sample	$T_m/^\circ\text{C}$	$\varepsilon_{r,m}$	$\tan \delta_m$	$\gamma$	$\Delta T_{\text{diffuse}}/\text{K}$
BSSnT-18-6.5	27	25,300	0.0040	1.7	4.4
BSSnT-Cu	19	12,900	0.0074	1.6	6.5
BSSnT-Mg	-11	4900	0.0119	1.9	21.4
BSSnT-Cu-Mg	-1	4700	0.0187	1.7	23.5

Figure 6 shows the temperature dependence of  $\varepsilon_r$  at different frequencies for BSSnT-18-6.5 bulk ceramics with different additives. The permittivity of BSSnT-18-6.5 with additions of MgO and CuO/MgO shows frequency dispersion around the permittivity peak, and the maximum relative permittivity decreases with increasing frequency, which confirms the relaxor behavior previously discussed.

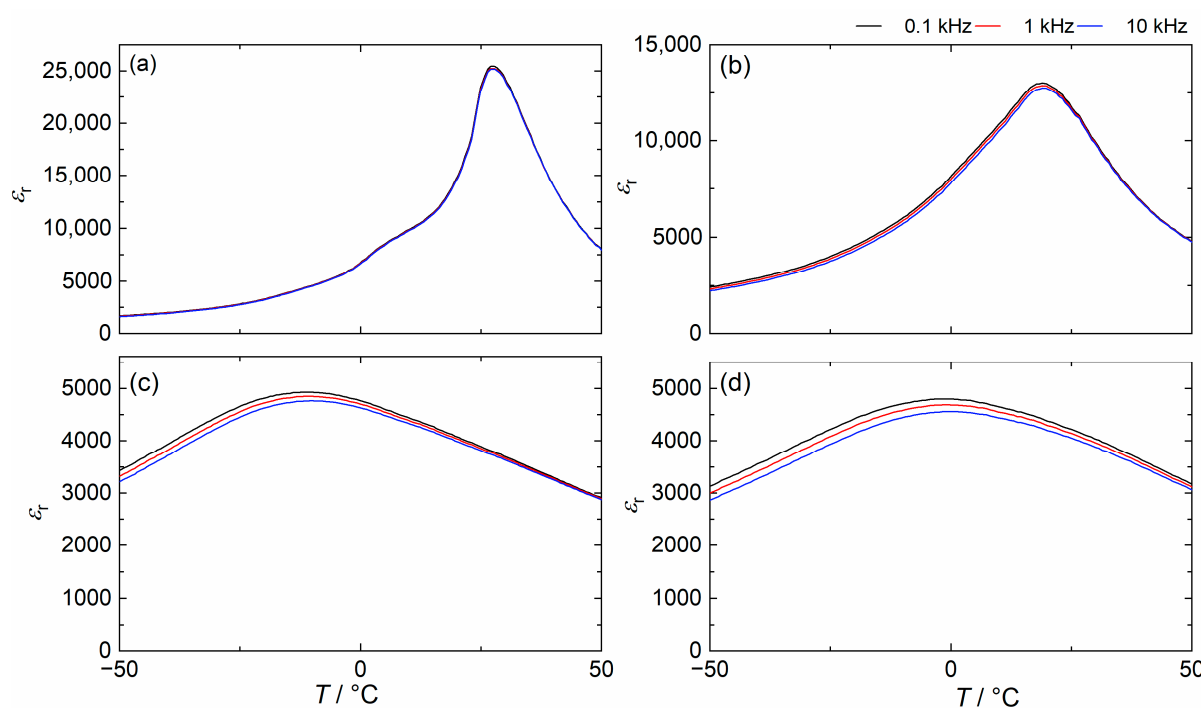


**Figure 6.** Temperature dependence of  $\epsilon_r$  measured at different frequencies for BSSnT-18-6.5 (a), BSSnT-Cu (b), BSSnT-Mg (c) and BSSnT-Cu-Mg (d).

### 3.5. Ferroelectric Properties

Figure 7 displays the electric field-dependent polarization of BSSnT-18-6.5 with different additives measured at electric fields varying from  $-2$  to  $2 \text{ V } \mu\text{m}^{-1}$  at  $-10, 20, 50, 80 \text{ } ^\circ C$  and  $10 \text{ Hz}$ . The polarization decreases for all compositions with increasing temperature, and the loops become slimmer and, finally, almost linear, indicating the transition of samples from the ferroelectric phase to the paraelectric phase. For better comparison, hysteresis loops of BSSnT-18-6.5 with different additives measured at  $20 \text{ } ^\circ C$  and  $10 \text{ Hz}$  are shown in Figure 8. By the addition of CuO and MgO, the hysteresis loops become narrower, indicating a decrease in ferroelectric hysteresis losses (see also Table 3). Additionally, the remanent polarization ( $P_r$ ) strongly decreases. According to the work by Su and Button [33], distortions due to oxygen vacancies lead to the formation of both electric and elastic dipoles. Their orientation causes domain-wall pinning and consequently reduced dissipation in the ferroelectric state. Moreover, according to Martirena and Burfoot [40], a reduction in the grain size affects ferroelectric properties by constraining the motion of domain walls, resulting in the behavior of each grain acting as a single domain. As grain boundaries can be additional pinning points for the motion of domain walls, walls move quite freely in giant grains and their motion is inhibited by a decrease in grain size. Additionally, the grain boundaries are considered low-permittivity regions and have poor ferroelectricity [44]. Thus, fine grains with more grain boundaries lead to a decrease in polarization. Since the additives induce oxygen vacancies [25,28] and the addition of MgO decreases the grain size significantly, the reduced ferroelectric properties can be understood as the combination of both effects. A summary of the ferroelectric data is listed in Table 3. Figure S3 shows the decrease in remanent polarization ( $P_r$ ) with increasing temperature, indicating that the samples underwent diffuse phase transition.

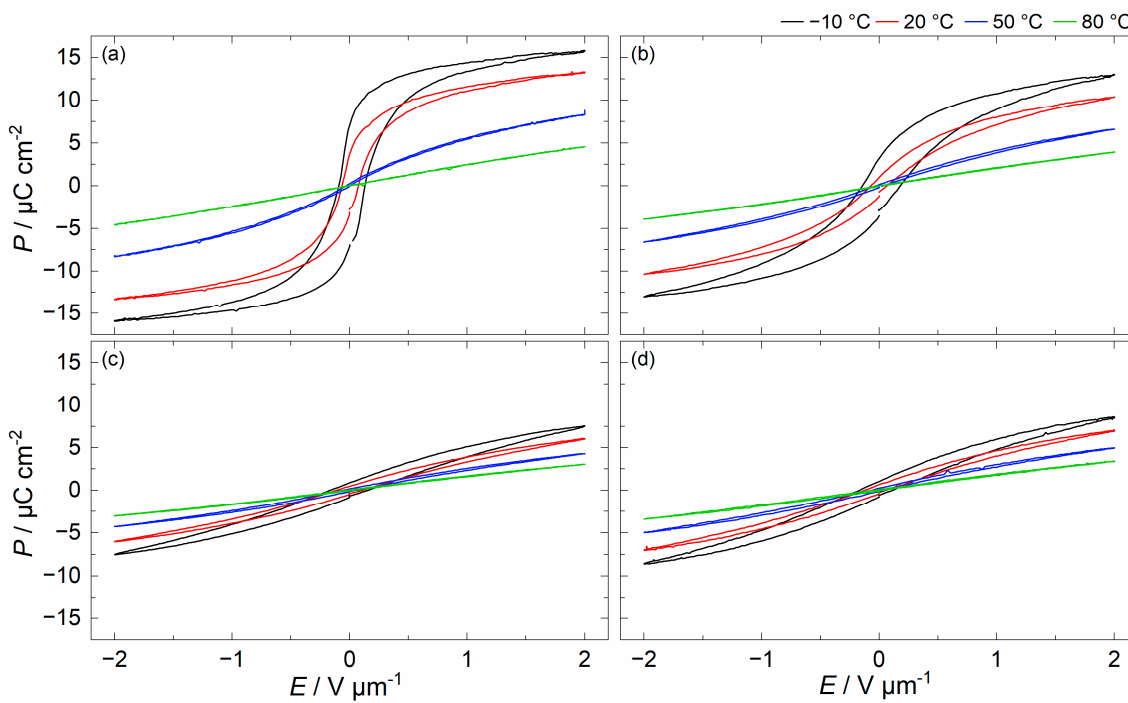


**Figure 7.** Hysteresis loops measured at  $-10, 20, 50, 80\text{ }^{\circ}\text{C}$  and  $10\text{ Hz}$  for BSSnT-18-6.5 (a), BSSnT-Cu (b), BSSnT-Mg (c) and BSSnT-Cu-Mg (d).

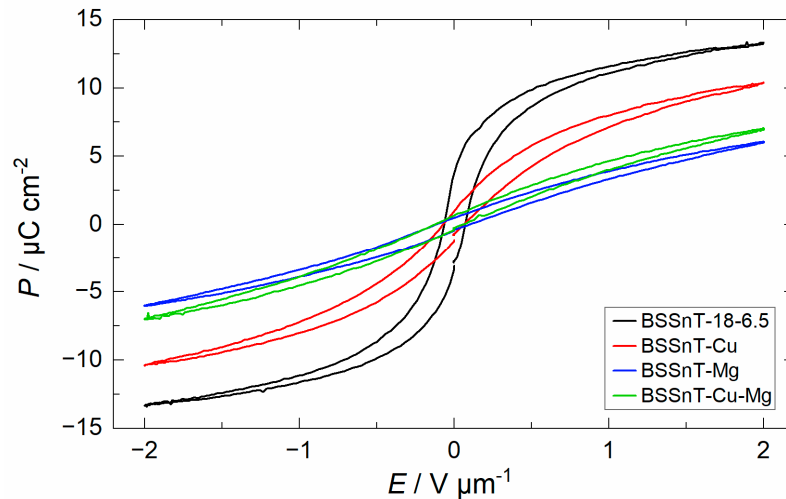


**Figure 8.** Hysteresis loops for BSSnT-18-6.5 with different additives measured at  $20\text{ }^{\circ}\text{C}$  and  $10\text{ Hz}$ .

**Table 3.** Compilation of maximum polarization ( $P_m$ ), remanent polarization ( $P_r$ ) and coercive field  $E_c$  for BSSnT-18-6.5 with different additives (measured at  $10\text{ Hz}$ ,  $2\text{ V }\mu\text{m}^{-1}$ ).

Sample	$P_m/\mu\text{C cm}^{-2}$	$P_r/\mu\text{C cm}^{-2}$	$E_c/10^{-2}\text{ V }\mu\text{m}^{-1}$
BSSnT-18-6.5	13.38	3.30	4.72
BSSnT-Cu	10.40	0.82	5.18
BSSnT-Mg	6.06	0.42	8.57
BSSnT-Cu-Mg	6.95	0.58	4.77

### 3.6. Electrocaloric Properties

The temperature-dependent electrocaloric effect (ECE) was measured directly in an environmental test chamber by using a fine-diameter thermocouple which was firmly attached to the samples by pressing them with a PTFE stamp. The results of the electrocaloric

temperature change ( $|\Delta T_{EC}|$ ), dependent on the temperature caused by the withdrawal of a comparatively low electric field of  $\Delta E = 2 \text{ V } \mu\text{m}^{-1}$ , are shown Figure 9. In addition, the electrocaloric properties of BSSnT-18-6.5 with different additives are summarized in Table 4. By adding CuO, MgO or CuO/MgO to BSSnT-18-6.5, the EC peaks become broader while the maximum of the ECE decreases drastically. The values of the heat capacities ( $c_p$ ) also become broader, and the visible peak in BSSnT-18-6.5 disappears as additives are introduced (Figure S4). Pure BSSnT-18-6.5 shows an electrocaloric temperature change ( $|\Delta T_{EC}|$ ) of  $>0.25 \text{ K}$  in a broad temperature range from 10 to  $60^\circ\text{C}$ . The addition of MgO strongly reduces the electrocaloric temperature change ( $|\Delta T_{EC}|$ ). However, the sample with the addition of MgO can withstand higher electric fields of up to  $\Delta E = 5 \text{ V } \mu\text{m}^{-1}$  during EC measurements due to the increased dielectric strength compared to pure BSSnT-18-6.5. In the latter, a maximum electrocaloric temperature change,  $|\Delta T_{EC}| = 0.27 \text{ K}$ , at  $30^\circ\text{C}$  was measured with almost no aberration within the temperature range from 5 to  $50^\circ\text{C}$  (Figure 10).

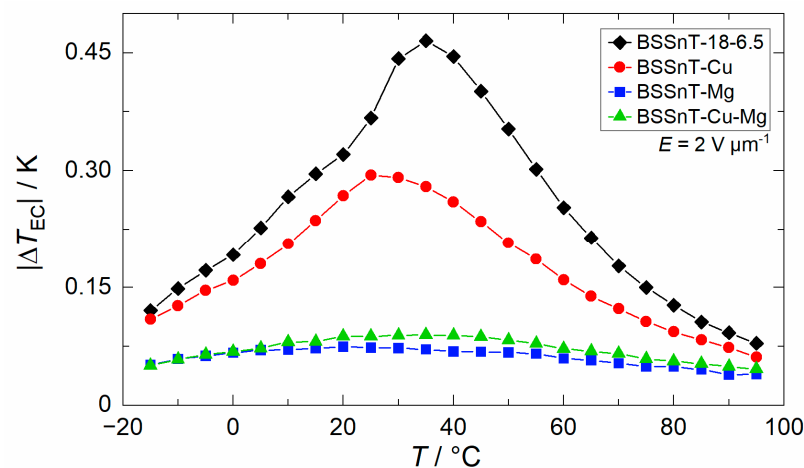


**Figure 9.** Electrocaloric temperature change ( $|\Delta T_{EC}|$ ) depending on temperature ( $T$ ) for BSSnT-18-6.5 with different additives measured at  $\Delta E = 2 \text{ V } \mu\text{m}^{-1}$ .

**Table 4.** Compilation of maximum electrocaloric temperature change ( $|\Delta T_{EC}|$ ) measured at an electric field change ( $\Delta E$ ) of  $2 \text{ V } \mu\text{m}^{-1}$ , corresponding temperature ( $T$ ), dielectric breakdown strength ( $E_{bd}$ ) and specific heat capacity ( $c_p$ ) at zero electric field.

Sample	T/°C	$ \Delta T_{EC} /\text{K}$	$E_{bd}/\text{V } \mu\text{m}^{-1}$	$c_p/\text{J kg}^{-1} \text{ K}^{-1}$
BSSnT-18-6.5	35	0.47	4.4	465
BSSnT-Cu	25	0.29	8.7	458
BSSnT-Mg	20	0.08	7.7	450
BSSnT-Cu-Mg	35	0.09	6.7	459

The correlation between the temperature of maximum ECE ( $T_{EC,max}$ ) and the temperature of maximum relative permittivity ( $T_m$ ) of BaTiO<sub>3</sub>-based materials (Figure 11) shows that the  $T_{EC,max}$  is usually 5 K above  $T_m$ . The addition of MgO increases the gap between the  $T_{EC,max}$  and  $T_m$  by 30 K. This can be explained by dielectric nonlinearity, i.e., a change in incremental permittivity in certain ferroelectric compositions undergoing a strong electric field [45].

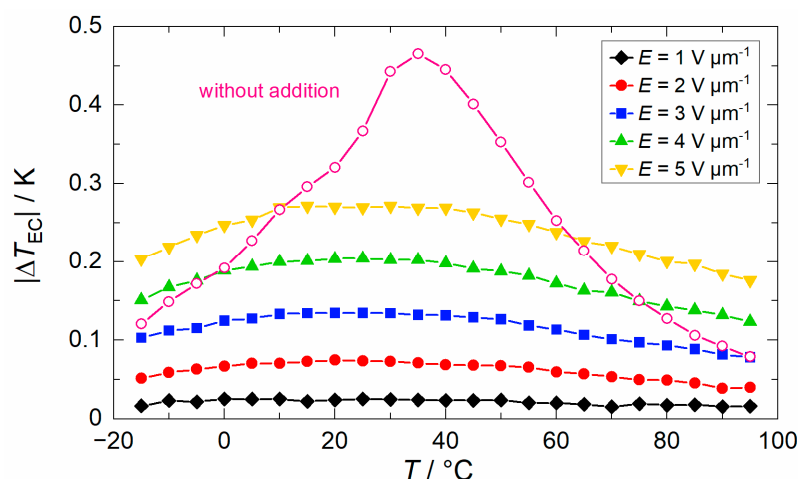


**Figure 10.** Electocaloric temperature change ( $|\Delta T_{EC}|$ ) depending on temperature ( $T$ ) for BSSnT-Mg measured under different electric fields (pink curve: electocaloric temperature change ( $|\Delta T_{EC}|$ ) depending on temperature ( $T$ ) for BSSnT-18-6.5 measured at  $\Delta E = 2 \text{ V } \mu\text{m}^{-1}$  as reference).

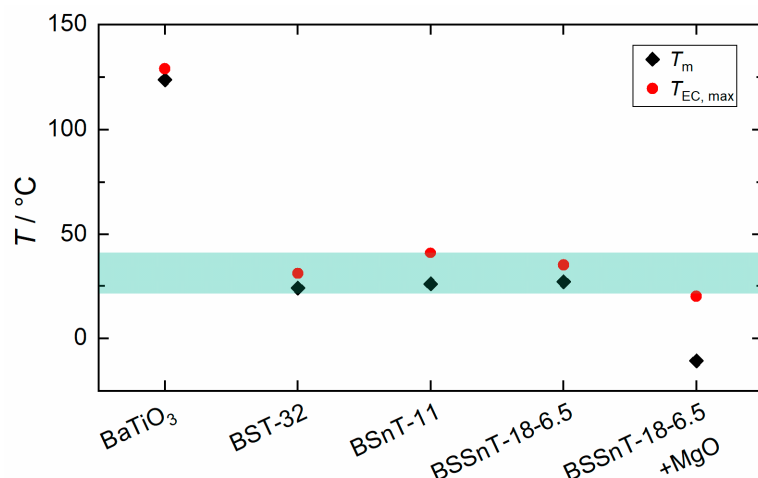


**Figure 11.** Compilation of temperature of maximum electrocaloric temperature change ( $T_{EC,max}$ ) measured at  $\Delta E = 2 \text{ V } \mu\text{m}^{-1}$  and temperature of maximum relative permittivity ( $T_m$ ) for bulk ceramics  $\text{BaTiO}_3$ ,  $\text{Ba}_{0.68}\text{Sr}_{0.32}\text{TiO}_3$  (BST-32),  $\text{BaSn}_{0.11}\text{Ti}_{0.89}\text{O}_3$  (BSSnT-11), [9] BSSnT-18-6.5 and BSSnT-18-6.5 with  $x_{\text{MgO}} = 1\%$ .

#### 4. Conclusions

In the present work, we investigate the influence of different additives on the lead-free electrocaloric material BSSnT-18-6.5 to allow its future application in multilayer ceramic components. By the addition of CuO, we successfully decreased the sintering temperature by 250 K from 1400 °C down to 1150 °C. However, its bimodal grain size distribution with coarse grains over 10 μm is not feasible for the fabrication of multilayer ceramic components with a ceramic layer thickness of around 40 μm. As for BSSnT-18-6.5 without additions, single grains could extend the inner electrode distance and thus allow electrical conduction through the grain boundaries [10]. The addition of MgO leads to a strong decrease in grain size from 40 μm to 0.4 μm. Moreover, a combination of both additives could be used to simultaneously decrease sintering temperatures and grain sizes. Although all additives lead to a decrease in the EC temperature change, the addition of MgO leads to a significant increase in dielectric strength, thus allowing the application of higher electric fields. Consequently, an EC temperature change of  $|\Delta T_{EC}| = 0.27 \text{ K}$  in a broad temperature range from 5 to 50 °C could be achieved for BSSnT-Mg. Our experiments show that EC properties are strongly dependent on the grain size of materials. Future investigations will

therefore focus on the influence of grain size on the ECE of BSSnT-Mg multilayer ceramic components and on tailoring the grain size to achieve an optimum high ECE and high dielectric strength in this lead-free material for EC applications.

**Supplementary Materials:** The following supporting information can be downloaded at: <https://www.mdpi.com/article/10.3390/inorganics11040151/s1>. Figure S1: FESEM-EDX mapping of BSSnT-Mg illustrating the occurrence of Mg-rich phase for this composition; Figure S2: Plot of  $\log(1/\varepsilon_r - 1/\varepsilon_{r,m})$  versus  $\log(T - T_m)$  and fitted curves at 1 kHz for BSSnT-18-6.5 ceramics with different additives; Figure S3: Temperature-dependent measurement of remanent polarization ( $P_r$ ) for BSSnT-18-6.5 with different additives measured at 2 V  $\mu\text{m}^{-1}$  and 10 Hz; Figure S4: Specific heat capacity ( $c_p$ ) depending on temperature ( $T$ ) for BSSnT-18-6.5 with different additives.

**Author Contributions:** Conceptualization, Z.L., C.M. and S.E.G.; methodology, Z.L. and C.M.; investigation, Z.L.; data curation, Z.L.; writing—original draft preparation, Z.L.; writing—review and editing, C.M. and S.E.G.; supervision, S.E.G. All authors have read and agreed to the published version of the manuscript.

**Funding:** This work was supported by the Fraunhofer Society in context of the lighthouse project “ElKaWe—Electrocaloric heat pumps” as well as by the Federal Ministry of Education and Research (BMBF) within the framework of the strategy and “Research for Sustainability” (FONA) [www.fona.de/en](http://www.fona.de/en). BMBF funding code: Elektrokalorik-Dioden-Kühlmodul (EKDM) (01LY1921A), accessed on 1 March 2023.

**Data Availability Statement:** Data are contained within the article or Supplementary Materials.

**Conflicts of Interest:** The authors declare no conflict of interest.

## References

- Correia, T.; Zhang, Q. *Electrocaloric Materials*; Springer: Berlin/Heidelberg, Germany, 2014.
- Fähler, S.; Rößler, U.K.; Kastner, O.; Eckert, J.; Eggeler, G.; Emmerich, H.; Entel, P.; Müller, S.; Quandt, E.; Albe, K. Caloric Effects in Ferroic Materials: New Concepts for Cooling. *Adv. Eng. Mater.* **2012**, *14*, 10–19. [[CrossRef](#)]
- Valant, M. Electrocaloric materials for future solid-state refrigeration technologies. *Prog. Mater. Sci.* **2012**, *57*, 980–1009. [[CrossRef](#)]
- Bai, Y.; Qin, S.; Nie, W.; Li, J.; Li, J.; Wang, H.; Qiao, L.; Guo, D. Influence of microstructure features on electrocaloric effect in ferroelectric ceramics. *Ceram. Int.* **2018**, *44*, 8263–8269. [[CrossRef](#)]
- Patel, S.; Kumar, M. Influence of grain size on the electrocaloric and pyroelectric properties in non-reducible BaTiO<sub>3</sub> ceramics. *AIP Adv.* **2020**, *10*, 85302. [[CrossRef](#)]
- Kartashev, A.V.; Bondarev, V.S.; Flerov, I.N.; Gorev, M.V.; Pogoreltsev, E.I.; Shabanov, A.V.; Molokeev, M.S.; Guillemet-Fritsch, S.; Raevskii, I.P. Study of the Physical Properties and Electrocaloric Effect in the BaTiO<sub>3</sub> Nano- and Microceramics. *Phys. Solid State* **2019**, *61*, 1052–1061. [[CrossRef](#)]
- Uršič, H.; Fulanović, L.; Vrabelj, M.; Kutnjak, Z.; Rožič, B.; Drnovšek, S.; Malič, B. Electrocaloric properties of 0.7Pb(Mg<sub>1/3</sub>Nb<sub>2/3</sub>)O<sub>3</sub>–0.3PbTiO<sub>3</sub> ceramics with different grain sizes. *Adv. Appl. Ceram.* **2016**, *115*, 77–80. [[CrossRef](#)]
- Vrabelj, M.; Uršič, H.; Kutnjak, Z.; Rožič, B.; Drnovšek, S.; Benčan, A.; Bobnar, V.; Fulanović, L.; Malič, B. Large electrocaloric effect in grain-size-engineered 0.9Pb(Mg<sub>1/3</sub>Nb<sub>2/3</sub>)O<sub>3</sub>–0.1PbTiO<sub>3</sub>. *J. Eur. Ceram. Soc.* **2016**, *36*, 75–80. [[CrossRef](#)]
- Lu, B.; Li, P.; Tang, Z.; Yao, Y.; Gao, X.; Kleemann, W.; Lu, S.-G. Large Electrocaloric Effect in Relaxor Ferroelectric and Antiferroelectric Lanthanum Doped Lead Zirconate Titanate Ceramics. *Sci. Rep.* **2017**, *7*, 45335. [[CrossRef](#)] [[PubMed](#)]
- Shebanov, L.A.; Borman, K. On lead-scandium tantalate solid solutions with high electrocaloric effect. *Ferroelectrics* **1992**, *127*, 143–148. [[CrossRef](#)]
- Xiao, D.Q.; Wang, Y.C.; Zhang, R.L.; Peng, S.Q.; Zhu, J.G.; Yang, B. Electrocaloric properties of (1 – x)Pb(Mg<sub>1/3</sub>Nb<sub>2/3</sub>)O<sub>3</sub>–xPbTiO<sub>3</sub> ferroelectric ceramics near room temperature. *Mater. Chem. Phys.* **1998**, *57*, 182–185. [[CrossRef](#)]
- Bell, A.J.; Deubzer, O. Lead-free piezoelectrics—The environmental and regulatory issues. *MRS Bull.* **2018**, *43*, 581–587. [[CrossRef](#)]
- Directorate-General for Environment; ECORYS; Ramboll. *Support for the Evaluation of Directive 2011/65/EU on the Restriction of the Use of Certain Hazardous Substances in Electrical and Electronic Equipment*; 2021. Available online: <https://op.europa.eu/en/publication-detail/-/publication/5b807311-9d93-11eb-b85c-01aa75ed71a1/language-en/format-PDF/source-278322860> (accessed on 28 March 2023).
- Zhao, C.; Yang, J.; Huang, Y.; Hao, X.; Wu, J. Broad-temperature-span and large electrocaloric effect in lead-free ceramics utilizing successive and metastable phase transitions. *J. Mater. Chem. A* **2019**, *7*, 25526–25536. [[CrossRef](#)]
- Bai, Y.; Zheng, G.-P.; Shi, S.-Q. Abnormal electrocaloric effect of Na<sub>0.5</sub>Bi<sub>0.5</sub>TiO<sub>3</sub>–BaTiO<sub>3</sub> lead-free ferroelectric ceramics above room temperature. *Mater. Res. Bull.* **2011**, *46*, 1866–1869. [[CrossRef](#)]
- Kumar, R.; Singh, S. Enhanced electrocaloric response and high energy-storage properties in lead-free (1 – x)(K<sub>0.5</sub>Na<sub>0.5</sub>)NbO<sub>3</sub>–xSrZrO<sub>3</sub> nanocrystalline ceramics. *J. Alloys Compd.* **2018**, *764*, 289–294. [[CrossRef](#)]

17. Tang, H.; Tang, X.-G.; Li, M.-D.; Liu, Q.-X.; Jiang, Y.-P. Pyroelectric energy harvesting capabilities and electrocaloric effect in lead-free  $\text{Sr}_x\text{Ba}_{1-x}\text{Nb}_2\text{O}_6$  ferroelectric ceramics. *J. Alloys Compd.* **2019**, *791*, 1038–1045. [[CrossRef](#)]
18. Molin, C.; Richter, T.; Gebhardt, S.E. Tailoring electrocaloric properties of  $\text{Ba}_{1-x}\text{Sr}_x\text{Sn}_y\text{Ti}_{1-y}\text{O}_3$  ceramics by compositional modification. *J. Eur. Ceram. Soc.* **2022**, *42*, 140–146. [[CrossRef](#)]
19. Molin, C.; Neumeister, P.; Neubert, H.; Gebhardt, S.E. Multilayer Ceramics for Electrocaloric Cooling Applications. *Energy Technol.* **2018**, *6*, 1543–1552. [[CrossRef](#)]
20. Fulanović, L.; Drnovšek, S.; Uršič, H.; Vrabelj, M.; Kuščer, D.; Makarovič, K.; Bobnar, V.; Kutnjak, Z.; Malič, B. Multilayer  $0.9\text{Pb}(\text{Mg}_{1/3}\text{Nb}_{2/3})\text{O}_3-0.1\text{PbTiO}_3$  elements for electrocaloric cooling. *J. Eur. Ceram. Soc.* **2017**, *37*, 599–603. [[CrossRef](#)]
21. Nair, B.; Usui, T.; Crossley, S.; Kurdi, S.; Guzmán-Verri, G.G.; Moya, X.; Hirose, S.; Mathur, N.D. Large electrocaloric effects in oxide multilayer capacitors over a wide temperature range. *Nature* **2019**, *575*, 468–472. [[CrossRef](#)]
22. Tunkasiri, T.; Rujijanagul, G. Dielectric strength of fine grained barium titanate ceramics. *J. Mater. Sci. Lett.* **1996**, *15*, 1767–1769. [[CrossRef](#)]
23. Cai, Z.; Wang, X.; Hong, W.; Luo, B.; Zhao, Q.; Li, L. Grain-size-dependent dielectric properties in nanograin ferroelectrics. *J. Am. Ceram. Soc.* **2018**, *101*, 5487–5496. [[CrossRef](#)]
24. Jo, W.; Ollagnier, J.-B.; Park, J.-L.; Anton, E.-M.; Kwon, O.-J.; Park, C.; Seo, H.-H.; Lee, J.-S.; Erdem, E.; Eichel, R.-A.; et al. CuO as a sintering additive for  $(\text{Bi}_{1/2}\text{Na}_{1/2})\text{TiO}_3-\text{BaTiO}_3-(\text{K}_{0.5}\text{Na}_{0.5})\text{NbO}_3$  lead-free piezoceramics. *J. Eur. Ceram. Soc.* **2011**, *31*, 2107–2117. [[CrossRef](#)]
25. Chen, T.; Zhang, T.; Wang, G.; Zhou, J.; Zhang, J.; Liu, Y. Effect of CuO on the microstructure and electrical properties of  $\text{Ba}_{0.85}\text{Ca}_{0.15}\text{Ti}_{0.90}\text{Zr}_{0.10}\text{O}_3$  piezoceramics. *J. Mater. Sci.* **2012**, *47*, 4612–4619. [[CrossRef](#)]
26. Sakabe, Y.; Wada, N.; Hiramatsu, T.; Tonogaki, T. Dielectric Properties of Fine-Grained  $\text{BaTiO}_3$  Ceramics Doped with CaO. *Jpn. J. Appl. Phys.* **2002**, *41*, 6922–6925. [[CrossRef](#)]
27. Boumous, S.; Belkhiat, S.; Kharchouche, F. MgO Effect on The Dielectric Properties of  $\text{BaTiO}_3$ . *Eng. Technol. Appl. Sci. Res.* **2019**, *9*, 4092–4099. [[CrossRef](#)]
28. Lin, Y.T.; Ou, S.F.; Lin, M.H.; Song, Y.R. Effect of MgO addition on the microstructure and dielectric properties of  $\text{BaTiO}_3$  ceramics. *Ceram. Int.* **2018**, *44*, 3531–3535. [[CrossRef](#)]
29. Derling, S.; Müller, T.; Abicht, H.-P.; Felgner, K.-H.; Langhammer, H.T. Copper oxide as a sintering agent for barium titanate based ceramics. *J. Mater. Sci.* **2001**, *36*, 1425–1431. [[CrossRef](#)]
30. Jeong, J.; Han, Y.H. Effects of MgO-Doping on Electrical Properties and Microstructure of  $\text{BaTiO}_3$ . *Jpn. J. Appl. Phys.* **2004**, *43*, 5373–5377. [[CrossRef](#)]
31. Chen, W.; Zhao, X.; Sun, J.; Zhang, L.; Zhong, L. Effect of the Mn doping concentration on the dielectric and ferroelectric properties of different-routes-fabricated  $\text{BaTiO}_3$ -based ceramics. *J. Alloys Compd.* **2016**, *670*, 48–54. [[CrossRef](#)]
32. Wang, X.; Liang, P.; Chao, X.; Yang, Z. Dielectric Properties and Impedance Spectroscopy of  $\text{MnCO}_3$ -Modified  $(\text{Ba}_{0.85}\text{Ca}_{0.15})(\text{Zr}_{0.1}\text{Ti}_{0.9})\text{O}_3$  Lead-Free Ceramics. *J. Am. Ceram. Soc.* **2015**, *98*, 1506–1514. [[CrossRef](#)]
33. Su, B.; Button, T.W. Microstructure and dielectric properties of Mg-doped barium strontium titanate ceramics. *J. Appl. Phys.* **2004**, *95*, 1382–1385. [[CrossRef](#)]
34. Uchino, K.; Nomura, S. Critical exponents of the dielectric constants in diffused-phase-transition crystals. *Ferroelectrics* **1982**, *44*, 55–61. [[CrossRef](#)]
35. Raddaoui, Z.; El Kossi, S.; Dhahri, J.; Abdelmoula, N.; Taibi, K. Study of diffuse phase transition and relaxor ferroelectric behavior of  $\text{Ba}_{0.97}\text{Bi}_{0.02}\text{Ti}_{0.9}\text{Zr}_{0.05}\text{Nb}_{0.04}\text{O}_3$  ceramic. *RSC Adv.* **2019**, *9*, 2412–2425. [[CrossRef](#)] [[PubMed](#)]
36. Skulski, R.; Wawrzala, P. The results of computerized simulation of the influence of dislocations on the degree of phase transition diffusion in  $\text{BaTiO}_3$ . *Phys. B Condens. Matter* **1997**, *233*, 173–178. [[CrossRef](#)]
37. Cai, W.; Fu, C.; Gao, J.; Lin, Z.; Deng, X. Effect of hafnium on the microstructure, dielectric and ferroelectric properties of  $\text{Ba}[\text{Zr}_{0.2}\text{Ti}_{0.8}]\text{O}_3$  ceramics. *Ceram. Int.* **2012**, *38*, 3367–3375. [[CrossRef](#)]
38. Mahajan, S.; Thakur, O.P.; Bhattacharya, D.K.; Sreenivas, K. Ferroelectric relaxor behaviour and impedance spectroscopy of  $\text{Bi}_2\text{O}_3$ -doped barium zirconium titanate ceramics. *J. Phys. D Appl. Phys.* **2009**, *42*, 65413. [[CrossRef](#)]
39. Buscaglia, V.; Buscaglia, M.T.; Viviani, M.; Mitoseriu, L.; Nanni, P.; Trefiletti, V.; Piaggio, P.; Gregora, I.; Ostapchuk, T.; Pokorný, J.; et al. Grain size and grain boundary-related effects on the properties of nanocrystalline barium titanate ceramics. *J. Eur. Ceram. Soc.* **2006**, *26*, 2889–2898. [[CrossRef](#)]
40. Martirena, H.T.; Burfoot, J.C. Grain-size effects on properties of some ferroelectric ceramics. *J. Phys. C Solid State Phys.* **1974**, *7*, 3182. [[CrossRef](#)]
41. Zhao, Z.; Buscaglia, V.; Viviani, M.; Buscaglia, M.T.; Mitoseriu, L.; Testino, A.; Nygren, M.; Johnsson, M.; Nanni, P. Grain-size effects on the ferroelectric behavior of dense nanocrystalline  $\text{BaTiO}_3$  ceramics. *Phys. Rev. B* **2004**, *70*, 24107. [[CrossRef](#)]
42. Mao, C.; Yan, S.; Cao, S.; Yao, C.; Cao, F.; Wang, G.; Dong, X.; Hu, X.; Yang, C. Effect of grain size on phase transition, dielectric and pyroelectric properties of BST ceramics. *J. Eur. Ceram. Soc.* **2014**, *34*, 2933–2939. [[CrossRef](#)]
43. Buscaglia, M.T.; Viviani, M.; Buscaglia, V.; Mitoseriu, L.; Testino, A.; Nanni, P.; Zhao, Z.; Nygren, M.; Harnagea, C.; Piazza, D.; et al. High dielectric constant and frozen macroscopic polarization in dense nanocrystalline  $\text{BaTiO}_3$  ceramics. *Phys. Rev. B* **2006**, *73*, 64114. [[CrossRef](#)]

44. Mudinepalli, V.R.; Feng, L.; Lin, W.-C.; Murty, B.S. Effect of grain size on dielectric and ferroelectric properties of nanostructured  $\text{Ba}_{0.8}\text{Sr}_{0.2}\text{TiO}_3$  ceramics. *J. Adv. Ceram.* **2015**, *4*, 46–53. [[CrossRef](#)]
45. Diamond, H. Variation of Permittivity with Electric Field in Perovskite-Like Ferroelectrics. *J. Appl. Phys.* **1961**, *32*, 909–915. [[CrossRef](#)]

**Disclaimer/Publisher's Note:** The statements, opinions and data contained in all publications are solely those of the individual author(s) and contributor(s) and not of MDPI and/or the editor(s). MDPI and/or the editor(s) disclaim responsibility for any injury to people or property resulting from any ideas, methods, instructions or products referred to in the content.